

# Magneto-elastic softening in cold-sprayed polycrystalline nickel studied by resonant ultrasound spectroscopy.

M. Janovská,<sup>1</sup> P. Sedlák,<sup>1</sup> M. Ševčík,<sup>1</sup> J. Cizek,<sup>2,3</sup> J. Kondas,<sup>4</sup> R. Singh,<sup>4</sup> J. Čupera,<sup>5</sup> and H. Seiner<sup>1</sup>

<sup>1</sup>*Institute of Thermomechanics, Czech Academy of Sciences, Dolejškova 5, 182 00 Prague 8, Czechia*

<sup>2</sup>*Institute of Plasma Physics, Czech Academy of Sciences, U Slovanky 2525/1, 182 00 Prague 8, Czechia*

<sup>3</sup>*Department of Materials Engineering, Faculty of Mechanical Engineering, Czech Technical University, Karlovo namesti 13, 120 00, Prague 2, Czechia*

<sup>4</sup>*Impact Innovations GmbH, Bürgermeister-Steinberger-Ring 1, Rattenkirchen, 84431, Germany*

<sup>5</sup>*Institute of Materials Science and Engineering, Brno University of Technology, Technická 2896/2 616 69 Brno, Czechia*

(\*Electronic mail: [hseiner@it.cas.cz](mailto:hseiner@it.cas.cz))

(Dated: 16 July 2025)

Cold-sprayed metallic deposits are additively manufactured materials containing high levels of compressive residual stress. Here we show that the presence and intensity of this stress can be analyzed using laser-ultrasonics, provided that the sprayed material is ferromagnetic and magnetostrictive, as in the case of pure nickel. Contactless resonant ultrasound spectroscopy is used to monitor the evolution of shear modulus and internal friction parameter of two polycrystalline Ni deposits with temperature over the Curie point, which enables a direct assessment of the strength of magneto-elastic softening that is known to be strongly stress-dependent. In addition, the proposed methodology is also shown to be suitable for in-situ observation of the recrystallization process in the vicinity of the Curie point, as well as inspecting the homogeneity of the residual stress level across the thickness of the cold-sprayed deposit. Finally, a methodology for room-temperature probing of the magnetoelastic coupling is proposed and tested on the examined materials.

## I. INTRODUCTION

Cold spray (CS) is a cost-efficient and rapid method for deposition of materials from feed-stock powders<sup>1–4</sup>. Initially regarded as a surface coating method, the absence of limitation on the achievable deposit thickness and other significant advantages of CS allowed its recent boom as an additive manufacturing method (CSAM)<sup>5–7</sup>. In the CS process, the powder particles are accelerated to supersonic velocities by a pressurized gas jet, and they undergo severe plastic deformation upon their impact onto the substrate or onto the preceding sprayed layers. The extreme-rate viscoplastic deformation triggers several phenomena that ultimately lead to the formation of very strong bond between the particles through metallurgical bonding and mechanical anchoring<sup>8–11</sup>. As a result, the final deposits exhibit a unique intensively-deformed microstructure as well as significant levels of residual compressive stress<sup>12–14</sup>. In turn, the residual stress affects the mechanical performance of the CS material: at low or moderate stress levels, its fatigue resistance is enhanced<sup>15–17</sup>, whereas, high levels of residual stress, may lead to delamination of the coatings or have a detrimental impact on shapes of additively-manufactured parts. For these reasons, the residual stress in CS deposits and its relation to the processing parameters have recently been extensively studied, utilizing a broad variety of experimental techniques, ranging from in-situ curvature measurements<sup>14</sup> and hole drilling<sup>18</sup>, to utilizing neutron diffraction<sup>19</sup>.

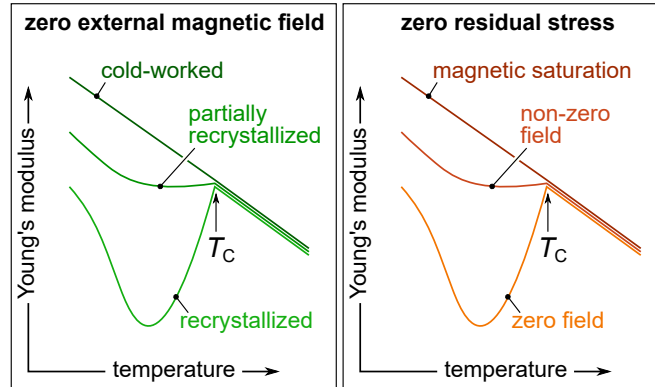


**FIG. 1:** An illustrative outline of the  $\Delta E$  effect in magnetostrictive materials. In zero magnetic field (left diagram), the level of residual stresses is indicated by the jump in the  $dE(T)/dT$  slope at the Curie point  $T_C$ , and the magnetoelastic softening of Young's modulus below this temperature. If there are residual stresses suppressing the magnetoelastic softening, the change of slope is weaker or absent. If the initially cold-worked material undergoes recrystallization, the level of residual stresses decreases (reaching zero for a fully recrystallized material), which is reflected by gradual amplifying of the  $\Delta E$  effect. If there are no residual stresses (right diagram), the  $\Delta E$  effect can be equivalently suppressed by performing the  $E(T)$  measurements in a magnetic field. In magnetic saturation, the magnetization vectors do not rotate with mechanical loading, and thus, the magnetostriction does not contribute to the strains and does not relax part of the stresses.

Ultrasonic methods are not typically used for such a task, despite their emerging employment in additive manufacturing technologies<sup>20–22</sup>. The main reason is that the elasto-acoustic constants in metals are rather low, and thus, it is difficult to distinguish the effects of residual stress on the acoustic parameters from those originating from defects, such as porosity, local imperfect bonding between the sprayed particles, or detectable volume fraction of amorphous phase due to increased density of grain boundaries<sup>23</sup>. An exception from this rule might be magnetostrictive ferromagnetic materials, in which the residual stresses affect the elasticity through magnetoelastic

coupling. In such materials, rotations of the magnetization vector under the action of ultrasonic vibrations lead to inelastic relaxation of a part of the strains, which results in effective softening of the elastic response, known as the  $\Delta E$  effect. The inelastic relaxation is suppressed by presence of residual stresses; as shown by Hubert et al.<sup>24</sup>, as low stresses as 3 MPa can have a measurable influence on the elastic modulus in polycrystalline nickel, and this effect becomes even more pronounced at elevated temperatures close to the Curie point. Figure 1 outlines the behavior reported and discussed for example in Refs. 25 and 26 (see also older works referred in the latter): in terms of its temperature dependence of the elastic modulus  $E(T)$ , cold-worked polycrystalline nickel in zero magnetic field behaves very similarly to the recrystallized polycrystalline nickel in magnetic saturation, that is, without any change of the  $dE(T)/dT$  slope at the Curie point. With relaxation of the residual stresses by annealing, this behavior changes, and a clear jump in the  $dE(T)/dT$  slope develops, resulting also in a significantly softer elastic behavior at the room temperature (RT). This means that the strength of the  $\Delta E$  effect may serve as a reliable indicator of the residual stresses, as well as for confirmation of their relaxation during annealing.

In this paper, we explore the ability of resonant ultrasound spectroscopy (RUS<sup>27–29</sup>) for assessing residual stresses in CS nickel coatings, and also the capability of this method for in-situ observation of the recrystallization process during which the residual stresses vanish and the  $\Delta E$  effect is restored. We show that this approach can also be used to evaluate the homogeneity of a CS deposit in terms of the residual stresses, proving that they are constant over the thickness; this is another valuable information from the point of view of considering CS as an additive manufacturing technology<sup>30</sup>. Finally, we discuss the main disadvantage of the proposed approach, which is the irreversible effect of the temperature-resolved experiments on the microstructure and the properties of the deposits. We show that these experiments can be, to some extent, replaced by room-temperature RUS measurements in magnetic field.

## II. EXPERIMENT

### A. Materials and sample preparation

Commercial-purity Ni powder Amperit 176.068 (H.C. Starck, Goslar, Germany) was used as the feedstock material. The powder range was measured as 15–44  $\mu\text{m}$  by laser scattering (d10–d90; Mastersizer 3000, Malvern Panalytical, UK) and its morphology was spherical (Figure 2), as a consequence of the used gas atomization production route. The nickel deposits were prepared using a high pressure ISS 5/11 cold spray system (Impact Innovations, GmbH, Germany). Nitrogen was used as the main process gas at 50 bar and 1100 °C. The stand-off distance was set to 30 mm and the robot arm traversal speed was 500 mm.s<sup>−1</sup>. Using a different number of passes, two deposits of thicknesses 6 mm and 11 mm were produced. The thinner (6 mm, denoted hereafter as CS1) deposit was sprayed onto a 110×50×10 mm<sup>3</sup> and the thicker deposit (11 mm, denoted hereafter as CS2) was sprayed onto a 50×50×10 mm<sup>3</sup> substrate; wrought commercial-purity aluminum was used as the substrate material in both cases. Using the Archimedes method, it was confirmed that both deposits had mass density very close to bulk nickel. In particular, the density determined for the CS1 and CS2 deposits were  $\rho = (8.72 \pm 0.04) \text{ g.cm}^{-3}$  and  $\rho = (8.83 \pm 0.04) \text{ g.cm}^{-3}$ , respectively, giving theoretical porosity of <1.5% and <0.3%. This also indicated slightly better compaction in the thicker deposit, probably due to a more intensive tamping effect triggered by the higher number of nozzle passes. To enable a comparison of the magnetoelastic behavior and the  $\Delta E$  for the examined CS deposits and a well-defined bulk material, additional experiments were done on a 4-mm sheet of low-carbon nickel (99.7% purity, alloy 201, ASTM B162; Bibus

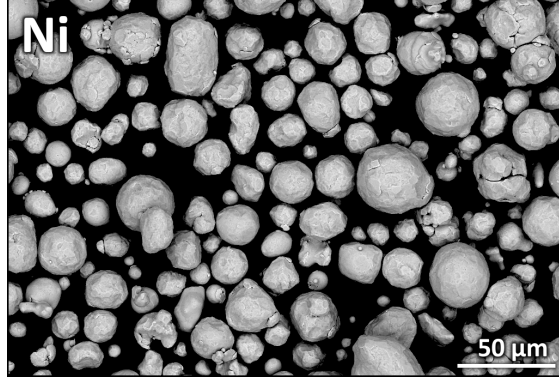


**FIG. 2:** Morphology of the Ni powder used as a feedstock for cold spraying.

Metals, Czech Republic). The sheet was hot rolled at 800 °C in the production, and had the mass density of bulk nickel (determined as  $\rho = (8.85 \pm 0.04) \text{ g.cm}^{-3}$ , a value used as the reference value for estimating the two CS porosities).

The microstructure of all three examined materials was analyzed using Carl Zeiss ULTRA Plus scanning electron microscope (Germany) equipped with a Nordlys Nano EBSD detector (Oxford Instruments, England). The analyses were performed on highly tilted samples (70° tilt) at an accelerating voltage of 20 kV and an aperture of 120  $\mu\text{m}$ . To estimate the amount of plastic strains in the grains, the kernel average misorientation (KAM) analysis was applied to the EBSD maps.

The samples for the ultrasonic analysis were cut from the central part of the CS1 and CS2 deposits and the reference rolled sheet in the form of prisms with dimensions of approximately  $4 \times 3 \times 2 \text{ mm}^3$ . At least three samples were cut from each type of material, which allowed us to confirm reproducibility of the results, as well as to prepare series of materials with different heat treatments, as explained below. The prismatic samples used for RUS analysis were ground on SiC papers using lapping/polishing machine Logitech CL50 (Logitech Ltd., Glasgow, United Kingdom) equipped with a jig to guarantee the parallelism of the opposite faces. The largest face of each sample was then mirror polished, as needed for the optical detection of vibrations in contactless RUS measurements. Additionally, smaller samples with dimensions approximately  $4 \times 3 \times 1.5 \text{ mm}^3$  were cut and similarly finished from the thicker (CS2) deposit from four locations differing in their distance from the deposit-substrate interface. These smaller samples were used to assess homogeneity of properties through the thickness of the deposit.

## **B. Resonant Ultrasound Spectroscopy**

### **1. Temperature-resolved RUS experiments**

A fully non-contact setup described in detail in Ref. 29 was used. The prismatic samples were placed into an evacuated chamber with a low-pressure ( $\sim 10 \text{ mbar}$ ) nitrogen atmosphere and a precise temperature control of  $\pm 1^\circ\text{C}$ . The vibrations of the sample were excited by a pulsed infrared laser focused onto the bottom face of the sample, and the time-domain response to this broadband excitation was recorded by a scanning laser vibrometer from the upper, mirror-polished face, and then processed using fast Fourier transform (FFT) to obtain the resonant frequencies (frequency range 200 kHz – 2 MHz) and the corresponding modal shapes.

Firstly, the RUS spectra were measured at room temperature (20 °C). At least 20 resonant fre-



quencies were reliably Identified for each sample. According to their modal shapes, the identified experimental resonant modes (frequencies  $f_n^{\text{exp}}$ ) were paired with calculated resonant modes (frequencies  $f_n^{\text{calc}}$ ) predicted by a numerical simulation described in detail in Ref. 29, using elastic constants of bulk polycrystalline nickel as initial guesses. These modes together with velocities of longitudinal ultrasonic waves in directions perpendicular to the individual faces of the samples were used as inputs for an inverse calculation of elastic constants. The calculation was based on minimization of the objective function

$$F(c_{ij}) = \sum_{n=1}^N \left( f_n^{\text{exp}} - f_n^{\text{calc}}(c_{ij}) \right)^2 \quad (1)$$

where  $N$  is the number of the reliably paired modes, and  $c_{ij}$  are the elastic constants. Transversal isotropy described by five independent elastic constants was assumed first for the CS1 and CS2 materials, and Young's moduli in the spray direction and the direction perpendicular to the spray direction were determined. Similar to the previous studies<sup>31,32</sup>, the deviation from isotropy was negligible as the difference of the two moduli was below 1 % for all studied samples. This said, both deposits were assumed as isotropic for further considerations. For the rolled sheet used as the reference material, elastic isotropy was assumed *a priori*, and the measured resonant spectrum was in a reasonable agreement with the spectrum calculated under this assumption.

Secondly, to inspect the differences in the magneto-elastic behavior of the materials, the RUS spectra for all samples were recorded in-situ during a single temperature cycle reaching 560 °C, i.e.,  $\sim 200^\circ\text{C}$  above the Curie temperature ( $T_C = 354^\circ\text{C}$  for pure Ni). The measurements were performed in a chamber equipped with a Joule-heating module, using a temperature step of  $20^\circ\text{C}$  and an average heating rate of  $2.8^\circ\text{C}.\text{min}^{-1}$ , including a 90s stabilization time for each measurement point. The materials response was then recorded during cooling with the same temperature step and the average cooling rate of  $2.5^\circ\text{C}.\text{min}^{-1}$ . Ten dominant resonant frequencies were traced for each sample along the temperature cycle, which enabled accurate ( $\pm 1$  GPa) and reliable evaluation of the temperature dependence of the isotropic shear modulus  $G(T)$  for each material. Changes of sample dimensions with the temperature due to thermal expansion and the corresponding changes in density were considered, assuming the linear expansion coefficients of pure nickel  $\alpha = 13 \times 10^{-6} \text{ K}^{-1}$ . Along the temperature cycle, the traced peaks were also used to determine the internal friction parameter  $Q^{-1}$  as

$$Q^{-1} = \frac{1}{N} \sum_{n=1}^N \frac{\text{FWHM}_n}{f_n}, \quad (2)$$

where  $\text{FWHM}_n$  stands for the full width at half maximum of the Lorentzian fit of the resonant peak at frequency  $f_n$ , and  $N$  is the number of used peaks ( $N = 10$  was used for all materials). It should be pointed out that the  $T_C$  temperature overlaps with the temperature range in which recrystallization of strongly cold-worked Ni can be expected<sup>33</sup>, and thus, the obtained  $Q^{-1}(T)$  temperature dependences were expected to be a superposition of magnetoelastic damping and recrystallization-related internal friction. Figure 3 shows examples of experimental RUS spectra used for this analysis and illustrates their evolution with temperature. It presents a comparison between a high-quality spectrum of the CS1 deposit in the initial as-sprayed condition and the spectrum of the same sample after heating it up above the recrystallization temperature and cooling back, resulting in softening of the material and a strong increase in internal friction. For the latter, the temperature of  $T = 160^\circ\text{C}$  (cooling run) was selected because it corresponded to the strongest magnetoelastic softening and highest internal friction, as discussed below. It is seen that

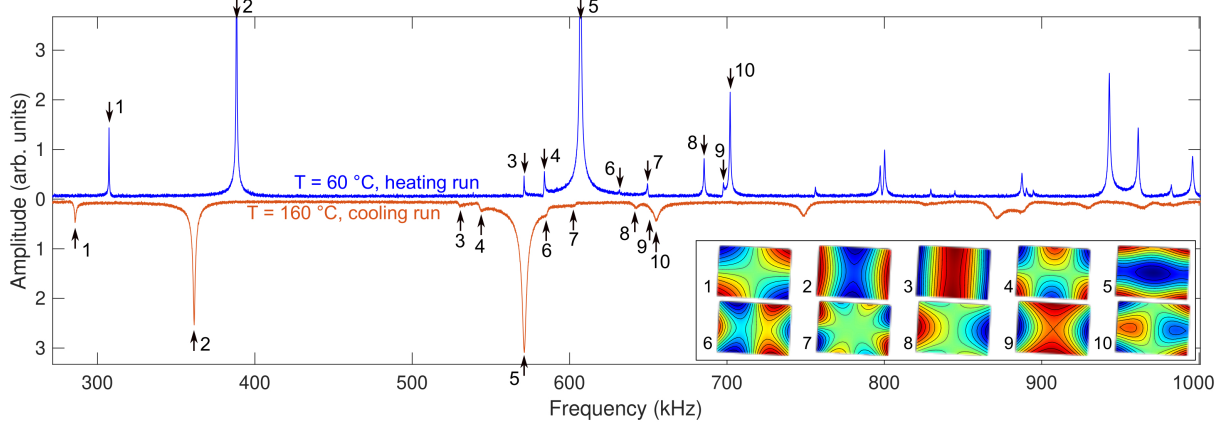


**FIG. 3:** The RUS spectrum for the CS1 sample in the initial condition (upright plot) and after the thermal cycle (upside-down plot). The peaks used for tracing the  $G(T)$  and  $Q^{-1}(T)$  evolutions are labeled with numbers 1 to 10; the modal shapes of these modes are shown in the bottom-right corner.

for this temperature the peaks considerably overlapped, and thus, the  $\text{FWHM}_n$  for equation (2) needed to be extracted by simultaneous fitting of the spectrum with a set of mutually overlapping Lorentzian masks. It is worth noting that the first ten resonant modes of an isotropic sample of the given geometry are dominantly determined by the shear modulus (according to the analysis reported in Ref. 34, the ratio of the sensitivity of the frequencies of these modes to the shear modulus versus the bulk modulus ranges from 15:1 to  $10^4$ :1), and thus, also the internal friction parameters extracted from the first ten modes can be understood as representing the shear internal friction. This makes the  $Q^{-1}$  obtained *via* the relation (2) very suitable for assessing the magnetoelastic coupling, which is a volume-preserving shear mechanism resulting from the rotation of the magnetization vector and magnetostriction.

Finally, all materials that underwent the  $\text{RT} \rightarrow 560^\circ\text{C} \rightarrow \text{RT}$  cycle were additionally annealed at  $700^\circ\text{C}$  for 96 hours to obtain reference samples with fully reversible and stable  $G(T)$  behaviors in the  $\text{RT} - 560^\circ\text{C}$  range due to their expected significant recrystallization, showing an amplified  $\Delta E$  effect. Let us note here that although the term  $\Delta E$  effect is commonly used in the literature, we will discuss changes in the shear modulus  $G$  in the following considerations, instead of the changes of Young's modulus  $E$ , because the shear modulus is more precisely determined by RUS for an isotropic material. The changes in Young's modulus  $\Delta E$  and the shear modulus  $\Delta G$  are closely interconnected, and can be expressed<sup>26</sup> as

$$\frac{\Delta G}{G} = \left( \frac{3G}{E} \right) \frac{\Delta E}{E}, \quad (3)$$

provided that the hydrostatic compressibility (the bulk modulus  $K$ ) remains constants, which holds approximately true for magnetoelastic softening. Since

$$\frac{3G}{E} = 1 + \frac{G}{3K}, \quad (4)$$

and since  $K$  is typically much larger than  $G$  ( $K = 250 \text{ GPa}$  vs.  $G = 76 \text{ GPa}$  for bulk polycrystalline nickel at the room temperature), the relative changes  $\Delta E/E$  and  $\Delta G/G$  are approximately equal to each other.

After the RT  $\rightarrow$  560°C  $\rightarrow$  RT cycle, as well as after the subsequent annealing, room-temperature RUS measurements were repeated, to keep track of the elastic properties evolution after the individual heat treatments.

## 2. *Magnetic field-resolved RUS experiments*

As an alternative approach to the temperature-resolved measurements, we further performed complementary measurements of the room-temperature (20 °C) evolution of shear moduli of the deposits CS1 and CS2 with magnetic field. For these experiments, the contactless experimental arrangement cannot be utilized, because the magnetic field creates a force acting on the sample, and thus, the rotation and motion of the sample must be prevented. This can be done in medium fields using the clamping force from ultrasonic transducers<sup>35</sup>, or in high magnetic field using an adhesive bonding between the transducers and the sample<sup>36</sup>. In both cases, the individual resonant frequencies might be shifted due to the contacts or the effective inertial mass of the transducers, but the qualitative evolution of the elastic response with magnetic field may still enable assessing the presence of residual stresses.

The experiments were performed between poles of an in-house built electromagnet, consisting of a water-cooled copper coil and a core made of ferritic steel. The electromagnet was designed for the maximum field of 0.4 T; in the used arrangement with the conventional RUS setup placed between the poles (Figure 4), the maximum reachable field was 0.26 T, which was sufficient for observing the field-induced changes of the elastic constants.

The sample in the RUS measurements was clamped between two miniature piezoelectric transducers VP-1093 (Valpey-Fisher Corp., Hopkinton, MA, USA). The excitation was performed by a chirp signal in frequency range from 20 kHz to 1 MHz, and the output signals were detected by the acquisition system in the time domain, averaged, and transformed into the final spectra by FFT in a frequency range 200 kHz – 1 MHz (which covers approximately the first 15 resonant frequencies for each sample). The clamping force from the transducers was enough to prevent rotations or other movements of the sample due to the magnetic field. Between the measurements at different field levels, the electromagnet was turned off to allow the coil to cool down. This ensured that the heat from the coil did not affect the temperature of the measured deposit.

In the field-resolved measurements, it was expected that the external magnetic field suppresses the  $\Delta E$  effect similarly as the residual stress does (see the analog between the field and the stress in Figure 1). Although this falls beyond the main scope of the paper, it shows a possibility how the main disadvantages of the temperature-resolved experiments can be circumvented. We show and discuss these results within the concluding results at the end.

## III. RESULTS AND DISCUSSION

### A. Microstructure characterization

The results of the scanning electron microscopy and the related KAM analysis are summarized in Figure 5. For the hot-rolled Ni sheet, large ( $\sim 100 \mu\text{m}$ ) grains were observed, mostly with a stripy substructure induced by the rolling, which results in relatively high misorientation angles in the KAM analysis. The presence of this substructure indicates the presence of dislocation walls in the rolled microstructure, and thus, residual stresses in this material were expected. After heating the material above  $T_C$ , the stripy contrast disappeared, indicating recovery and/or recrystallization,

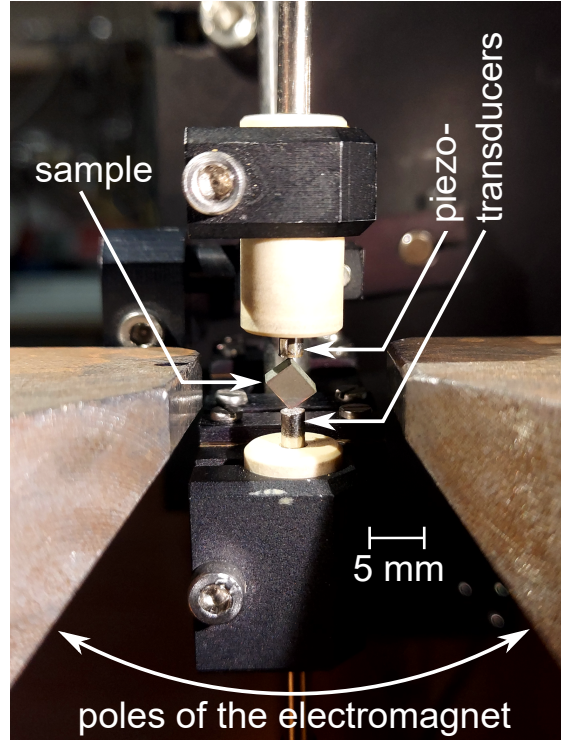


**FIG. 4:** The experimental arrangement for field-resolved RUS measurements. The sample is clamped along its body diagonal, which prevents its rotation or motion due to increased magnetic field.

but without any visible change of the grain size. The distribution of the KAM angles became much narrower and closer to zero, as expected for a material recovering residual stresses. With the long-term annealing at 700 °C, this process further continued, but the resulting changes in the SEM images as well as in the KAM curve were much less pronounced than between the initial condition and the condition after the RUS temperature cycle. In other words, the analysis confirmed the rolled sheet to be a suitable reference material that undergoes a transition from plastically deformed to recovered (or recrystallized) in the two subsequent heat treatments.

For the thinner CS1 deposit, the initial condition showed a typical fine-grained CS microstructure, documenting severe plastic deformation of the feedstock particles upon impact. This was further confirmed by the wavy arrangement of the refined grains as well as by the very broad distribution of the KAM angles. A bimodal grain size was observed, with chains of fine grains formed along the particle rims and relatively bigger grains retained in the particle centers, a consequence of the extreme plastic deformation during the particle impact<sup>37</sup>. With the temperature cycle during the RUS measurement, the microstructure became mostly recrystallized, with numerous micrometer-sized grains persisted, but with the wavy pattern being fully erased by the newly grown recrystallized grains. After annealing at 700 °C, a further grow of the recrystallized grains was observed, as confirmed also by the KAM analysis.

For the thicker CS2 deposit, the initial microstructure had a bimodal character, with several areas filled with ultra-fine grains, but other consisting mainly of larger grains. This can be interpreted as a result of partial dynamic recrystallization during the spraying process<sup>38</sup>. This deposit was sprayed onto a smaller substrate with higher frequency of spraying passes, which resulted in higher temperatures in the deposit during the process. The bimodality of the microstructure in the initial condition can be seen also from the KAM curve, which exhibits a pronounced peak at small



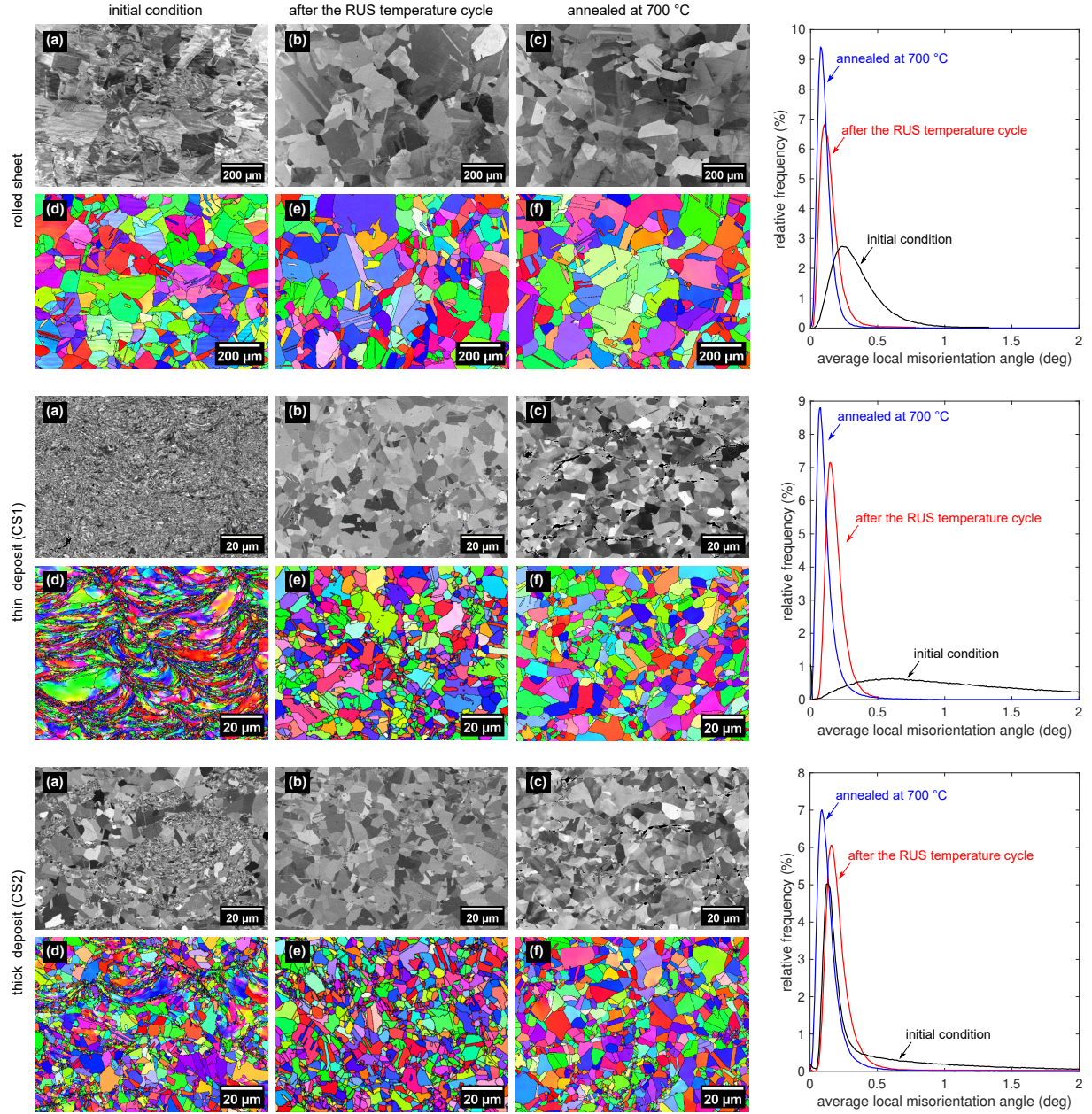


**FIG. 5:** Characterization of microstructures of the examined materials. For each material, electron channeling contrast SEM micrographs (a,b,c) and EBSD maps (d,e,f) are shown. The micrographs and maps refer to three conditions for each material: the initial microstructure (a,d); the microstructure after heating the material above the Curie point and back (b,e); and after 96 h annealing at 700 °C (c,f). Average misorientation angles of the lattice inside the grains (from the KAM analysis) in the given three microstructures for each material are shown in the right column graphs. Note the different scalebars in the reference rolled sheet and the CS-ed deposits.

angles (as would be typical for a recrystallized material), as well as a long 'tail' towards higher angles, representing the refined, heavily plastically deformed grains. This 'tail' disappeared after the first temperature cycle, which corresponds to the disappearance of the smallest grains as well as of the wavy patterns, clearly seen in the SEM micrographs. Similarly as for CS1, the final an-

**TABLE I:** Average grain area (in  $\mu\text{m}^2$ ) extracted from the EBSD maps in Figure 5

	initial condition	after the RUS temperature cycle	annealed at 700 °C
rolled sheet	$9.1 \times 10^3$	$10.6 \times 10^3$	$11.5 \times 10^3$
CS1	2.5	9.65	29.15
CS2	5.37	5.71	21.32

nealing in CS2 resulted in a narrower KAM angle distribution and more completely recrystallized microstructure seen in the micrographs.

A quantitative insight into the recrystallization process in the examined materials can be obtained from the evolution of average grain size (measured by the average grain area in the micrograph) presented in Table I. It is seen that only for the CS1 material the RUS temperature cycle resulted in a pronounced grain growth. This means that only for this material, the residual stresses and the energy of the impact-induced defects (grain refinement, substructuring) were strong enough to trigger massive recrystallization. Further heating for this materials stimulated further grain growth, and, as a result, the most completely recrystallized microstructure among all studied materials was obtained for CS1 after the final annealing at 700 °C. In contrast, nearly no grain growth was observed for the rolled sheet, which indicated that this material did not undergo recrystallization, and the residual stresses were relaxed by recovery of the grain substructure. For the CS2 coating, with lower density of defects, and thus, with lower driving force on the recrystallization, the main grain growth was obtained during annealing at 700 °C. During the RUS temperature cycle, the smallest grains in CS2 disappeared, but the rest of the microstructure, already partially recrystallized from the production, remained intact, resulting in just small increase in the grain size on average.

In summary, the microstructural observations confirmed that the three chosen materials represent polycrystalline nickel with three different levels of plasticity-induced grain refinement and substructuring, and presumably also of the residual stresses, and that these materials undergo different microstructural processes during the used heat treatments. That is, it was confirmed that this set of materials was suitable for analyzing the ability of RUS experiments to monitor these features.

## B. Laser-based RUS

### 1. Room-temperature elastic constants

Room-temperature elastic constants of all studied materials and in all discussed conditions are listed in Table II. Although all materials are polycrystalline nickel with zero to very small (<1.5%) porosity, it is observed that these constants vary significantly. As expected, the softest elastic behavior ( $G < 75$  GPa after both the RUS temperature cycle and the annealing) is observed for deposit CS1 that underwent the most complete recrystallization, and in which the strongest  $\Delta E$  effect can be expected. However, other observed differences are not that easy to interpret. For example, in the initial condition, the CS1 deposit is the softest among all materials, even though it can be, based on the above microstructural analysis, expected to have the highest level of residual stresses, and thus, the most suppressed  $\Delta E$  effect. As it will be obvious from the temperature-resolved RUS measurements reported below, this is partially because of the high density of defects, and this artificial softening disappears with recrystallization; but partially, this may be also because



**TABLE II:** Room temperature elastic constants of nickel sheet and CS1 and CS2 deposits after different heat treatment.

	rolled sheet		CS1		CS2	
	$G$ (GPa)	$E$ (GPa)	$G$ (GPa)	$E$ (GPa)	$G$ (GPa)	$E$ (GPa)
initial condition	80.9	212	77.7	203	79.8	209
after the RUS temperature cycle	79.8	210	73.8	195	78.2	205
annealing at 700 °C	80.5	212	74.5	196	77.0	202
accuracy	$\pm 0.7$	$\pm 2$	$\pm 0.7$	$\pm 2$	$\pm 0.7$	$\pm 2$

of the porosity. In other words, the room-temperature elasticity information itself is insufficient for any discussion of the changes occurring in the microstructure with the heat treatment.

## 2. Temperature behavior

A more detailed insight into the magnetoelastic behaviors of the examined materials can be obtained through temperature-resolved RUS measurements, resulting in  $G(T)$  and  $Q^{-1}(T)$  curves. For the rolled sheet, these curves are shown in Figure 6(a). The effect of magnetism is clearly seen in both subfigures. The Curie temperature  $T_C$  causes a sharp change in the  $dG(T)/dT$  slope, as the magnetoelastic softening is active only below this temperature. The change is sharper during the cooling run, confirming that the relaxation of internal stresses during the temperature cycle led to enhancing the  $\Delta E$  effect. However, even this change of slope is much less pronounced than what was reported in the literature for fully annealed materials<sup>24,25</sup>, and it can be therefore concluded that the used temperature cycle resulted only in a partial relaxation of the residual stresses in the sheet. The effect of  $T_C$  on the internal friction is also obvious, as the para-to-ferromagnetic transition triggers the strong magnetoelastic damping below the Curie point. Surprisingly, the damping is stronger in the initial condition than after the partially release of the residual stresses. This suggests that in the initial condition, there might be more complex coupling between the stripy substructure of the grains and the magnetic domains, since very fine magnetic domains may strengthen the magnetoelastic damping<sup>35</sup>. For both the heating and the cooling run, however, the  $Q^{-1}(T)$  curves exhibit identical features. There is a maximum of the damping at about 100 °C, which probably results from an interplay between temperature evolutions of the magnitude of magnetostriction and of the magnetocrystalline anisotropy. And, above  $T_C$  the internal friction continuously increases, as expected for any polycrystalline metal because of easier activation of nonmagnetic relaxation processes (dislocations, point defects, grain boundary sliding<sup>39,40</sup>) with increasing temperature.

For the deposit CS1 (Figure 6(b)), much more complex behavior is observed for both  $G(T)$  and  $Q^{-1}(T)$ . No sharp change of the slope is observed for the shear modulus at  $T_C$  during the heating run, which indicates the  $\Delta E$  effect is completely suppressed in the initial condition. Instead, a relative stiffening with respect to the low-temperature  $G(T)$  linear trend is observed upon further heating, terminating at approximately 480 °C. This stiffening is accompanied with a rather broad internal friction peak. Both the stiffening and the peak indicate that recrystallization occurs in this temperature range. In the initial condition, the severe plastic deformation resulted a high density of grain boundaries and defect-supersaturated lattice inside the grains<sup>41</sup>. The amorphous regions inside of the boundaries as well as the heavily distorted lattice have softer elastic constants, and thus, weak elastic stiffening is a common feature accompanying recrystallization<sup>42–44</sup>. This

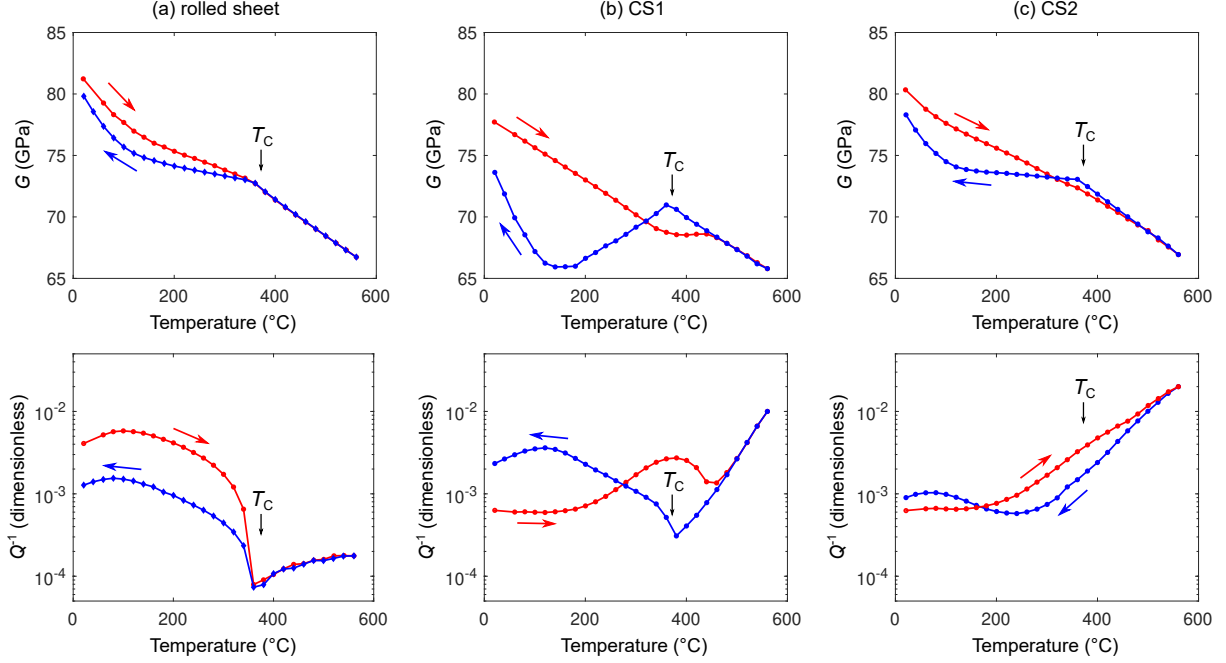


**FIG. 6:** Magnetoelastic behavior in all studied materials presented in the form of  $G(T)$  and  $Q^{-1}(T)$  curves. (a) rolled Ni sheet used as a reference bulk material; (b) thinner CS1 deposit with strong grain refinement and wavy microstructure indicating severe plastic deformation; (c) thicker CS2 deposit, in which partial recrystallization occurred during the spraying process.

explains why the CS1 material is not elastically the stiffest in the initial condition, although the  $\Delta E$  effect in it is the most strongly suppressed. The cooling curves for both  $G(T)$  and  $Q^{-1}(T)$  are then very similar to those for the rolled sheet, but with a much sharper change of the  $dG(T)/dT$  slope at the Curie point, which indicates a strong  $\Delta E$  effect in the recrystallized microstructure. The cooling  $G(T)$  curve clearly resembles theoretically predicted curves for polycrystalline nickel with low residual stresses, reported in Ref. 24, as well as experimental curves for partially recrystallized cold-worked materials reported in Ref. 25.

For the deposit CS2 (Figure 6(c)), the effect is qualitatively similar as for CS1, but with several important quantitative differences. Most importantly, there already is some weak slope change in  $G(T)$  at the Curie point during the heating run, which is in perfect agreement with the partially recrystallized structure in the initial condition. Then, the increase of  $G$  above  $T_C$  due to recrystallization is very weak (observable, but below the experimental accuracy level). In the cooling, a stronger but still quite weak change of the slope is observed at  $T_C$ , which indicates that the residual stresses were not significantly released during the cycle. On the  $Q^{-1}(T)$  curve, the sharp drops at  $T_C$  are not observed, which reveals that the recrystallization was triggered in this temperature range both during the heating and the cooling runs. Because of the minor volume fraction of the small grains and probably also a smaller density of other defects, the recrystallization progressed much slower than in CS1, and thus, the recrystallization peak overlapped with the para-to-ferromagnetic transitions.

To obtain stable  $G(T)$  and  $Q^{-1}(T)$  curves not affected by time-dependent features related to the recrystallization for reference, all three materials were annealed at 700 °C for 96 hours. Then, the RT  $\rightarrow$  560°C  $\rightarrow$  RT RUS experiments were repeated. As expected, in this temperature range,

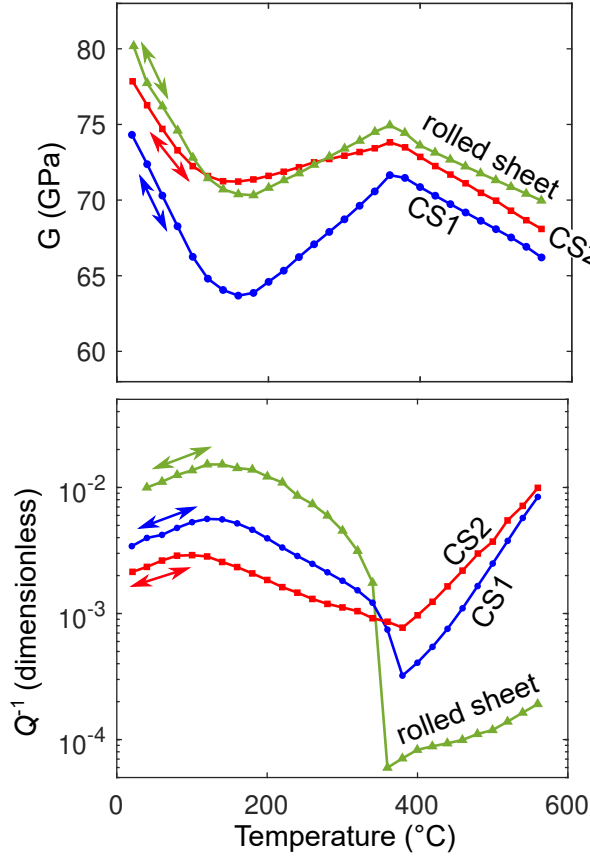


**FIG. 7:** Stable  $G(T)$  and  $Q^{-1}(T)$  behaviors of materials annealed at 700 °C for 96 hours.

the  $G(T)$  and  $Q^{-1}(T)$  became fully reversible. The behaviors are summarized in Figure 7. It is seen that all  $G(T)$  curves adopted shapes typical for the  $\Delta E$  effect, with the minimum at  $G(T)$  (corresponding approximately to the maximum at  $Q^{-1}(T)$ ) marking the temperature where the anelastic contribution to the vibrations by magnetostriction is the strongest. Despite the annealing, however, significant differences are still seen among the curves. The weakest effects of  $T_C$  are observed for the deposit CS2, indicating that this material retained the highest level of residual stresses. For the rolled sheet, the effect on  $G(T)$  is somehow stronger, while the effect on  $Q^{-1}(T)$  is very strong. Considering the  $\sim 10^3 \times$  larger grain size and zero porosity for the sheet compared with the CS deposits, this probably indicates that the ferromagnetic domain walls are easier to move in the material, leading to stronger damping. This material did not undergo recrystallization during the annealing, and thus, the level of residual strains, as well as the  $G(T)$  and  $Q^{-1}(T)$  curves for it are quite similar as those measured during the cooling run of the first  $RT \rightarrow 560^\circ\text{C} \rightarrow RT$  cycle before the annealing. Finally, the strongest effect is observed for the most completely recrystallized CS1 deposit, for which also the elasticity at the room temperature is the softest (Table II). Let us point out, however, that the relative drop in  $G$  between the Curie point and its minimum, which is approximately 20% is still much weaker than for fully recrystallized (annealed at 1300 °C) polycrystalline nickel reported in Ref.25, for which  $E$  drops by more than 35% (notice that the drops in  $E$  and  $G$  should be comparable, according to Equations (3) and (4)).

### 3. *Confirming homogeneity of residual stresses*

Since the above results prove that the magnetoelastic features on the  $G(T)$  and  $Q^{-1}(T)$  curves are sensitively dependent on the plastic strain accommodated in the microstructure, and on the related residual stresses, the presented approach can be used to compare different locations in the deposit. For this purpose, a set of samples covering the entire thickness of the deposit CS2 was prepared. Each of these samples was then subjected to the  $RT \rightarrow 560^\circ\text{C} \rightarrow RT$  temperature cycle with in-situ RUS characterization. The result is shown in Figure 8. It is seen that the  $G(T)$  curves for all samples are identical to each other within the experimental accuracy, proving a perfectly constant profile of residual stresses over the thickness of the deposit. A slight deviation in the  $Q^{-1}(T)$  curve is seen for the sample from the region closest to the free surface of the deposit (sample 1), where the internal friction is weaker at the very beginning of the temperature cycle. As this deviation is not reflected in the  $G(T)$  curve, it most probably corresponds to some internal friction mechanism with much longer relaxation times than magnetoelasticity, such as dislocation damping or grain boundary sliding<sup>39,40</sup>. These mechanisms can be somehow amplified in layers deeper in the deposit, where grains could be more distorted due to the tamping effect. However, the deviation is of the order of  $10^{-3}$ , and does not affect the further evolution of  $Q^{-1}(T)$  with the temperature cycle, where the curves are identical for all samples, documenting the same progress of partial recrystallization and the same magnetoelastic damping.

## IV. CONCLUDING REMARKS

The presented results confirm that the magnetoelastic coupling and the related  $\Delta E$  effect can serve as suitable indicators of residual stress levels in ferromagnetic cold-sprayed deposits, and that the RUS characterization can be used as a tool for monitoring their evolution. Using the laser-based modification of RUS, we were able to analyze not only the shear modulus changes, but also the internal friction, which allowed us to identify, for example, the temperature range in which the recrystallization occurs. The  $G(T)$  and  $Q^{-1}(T)$  curves clearly illustrated the differences between the CS1 and CS2 deposits, where the latter was partially recrystallized directly from the spraying process. The differences were seen not only in the as-sprayed behavior, where the  $\Delta E$  effect in CS1 was completely suppressed, but also from the reversible behavior after the medium-temperature annealing, where CS1 displayed signs of more complete recrystallization than CS2. The as-sprayed behavior enabled also assessing the homogeneity of the thick deposit CS2, as the identical  $G(T)$  and  $Q^{-1}(T)$  curves for various samples from this deposit confirmed that there where identical microstructural processes taking place in these samples during the thermal cycle, from which one can deduce that also the initial levels of residual stresses in samples from different distances from the substrate were identical. In principle, moreover, the obtained  $G(T)$  curves may allow for quantitative determination of the levels of residual stress in the material, utilizing the theoretical model of the magnetoelastic interaction developed in Ref.24. For cold-sprayed deposits, however, it must be taken into account that the variations of  $G$  are also given by recrystallization-induced stiffening, and that the macroscopic elastic moduli are also affected by porosity or the interconnection between the sprayed particles. As a result, the  $G(T)$  dependence can be more complicated than what predicted by the aforementioned model; the quantitative assessment of the residual stress levels would, thus, require a prior calibration by some more direct, independent method.

Another disadvantage of the applied approach is obviously in the overlapping between the temperature cycle reaching above the Curie point  $T_C$ , which is required for visualizing the strength

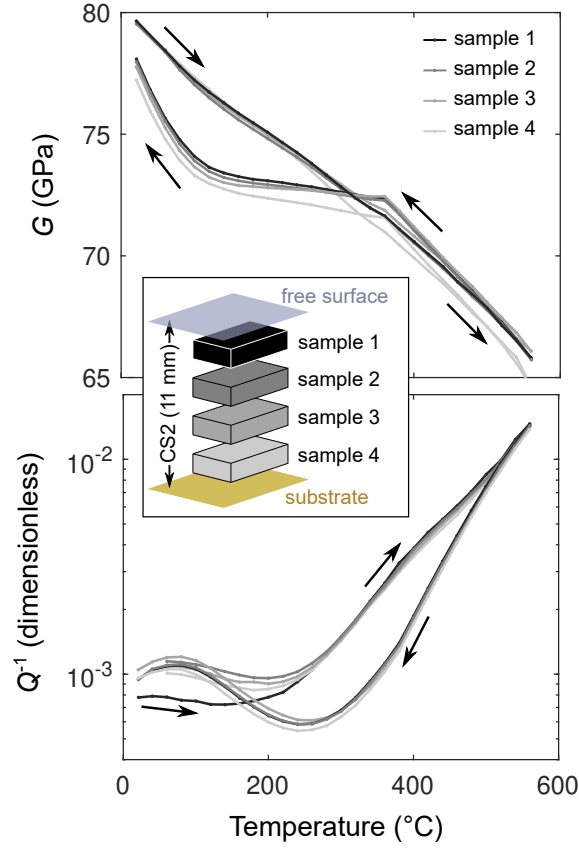


**FIG. 8:**  $G(T)$  and  $Q^{-1}(T)$  curves for temperature cycles reaching above  $T_C$  for four samples cut from the thick deposit CS2; these samples represent different locations across the thickness of the deposit. The identical  $G(T)$  behaviors in all these samples confirm the homogeneity of residual stresses in the deposit.

of the  $\Delta E$  effect, and the temperature interval for recrystallization of the CS deposits. This could be overcome by doing the RUS experiments in a controlled external magnetic field, owing to the equivalence between the field and the residual stresses, as outlined in Figure 1. This approach might be used also for additively manufactured CS parts of complex shapes, where field-resolved RUS measurements would enable confirming or refuting the presence of residual stresses in the given part, or verifying the repeatability of the manufacturing process by comparing the  $\Delta E$  effect in series of geometrically identical CS parts.

As a proof of this concept, we performed field-resolved RUS experiments on samples of CS1 and CS2 deposits, each in the as-deposited condition, and after the final heat treatment. The results are shown in Figure 9. While the absolute values of  $G(B)$  can be biased by the magnetic forces acting on the sample, and possibly also by other effects resulting from the contact between the transducers and the sample<sup>45,46</sup>, the evolutions show exactly the expected behaviors. All materials exhibit stiffening originating from suppressing the  $\Delta E$  effect, and the effect is the strongest for weak-to-intermediate fields, while above 0.2 T the materials are already close to magnetic saturation and  $G(B)$  converges to a constant value. In both deposits, the effect of the field is stronger for the annealed materials, confirming that in the as-deposited materials, the  $\Delta E$  effect is reduced due to residual strains.

Taking into account the technical difficulties of performing the experiments in a magnetic field,

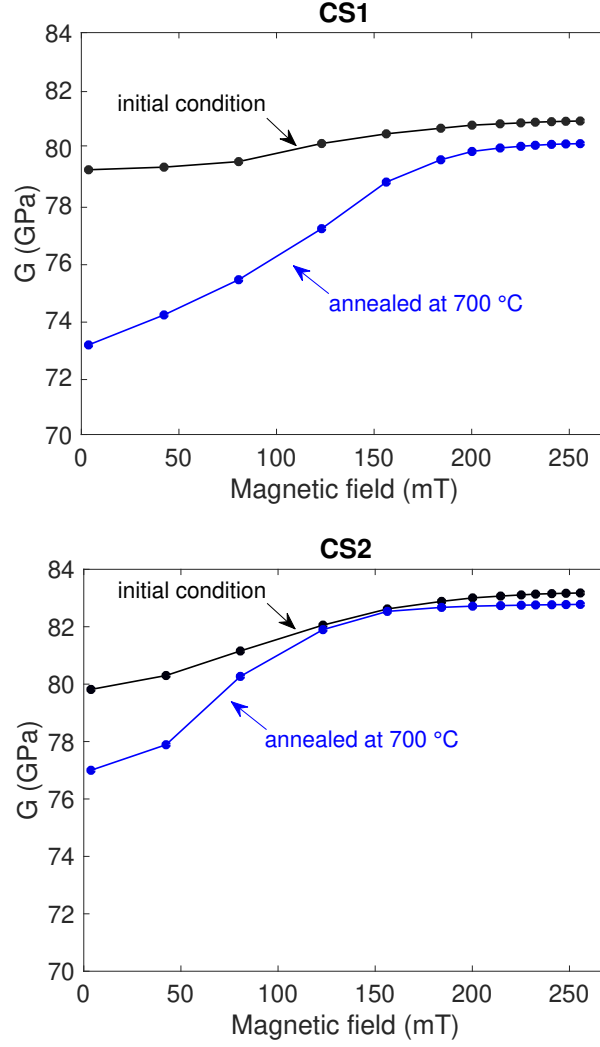


**FIG. 9:** Room-temperature shear moduli of the deposits CS1 and CS2 measured in magnetic field, clearly illustrating the different effects of the field on materials with different microstructures and different levels of residual stresses. Notice that the zero-field values of  $G$  are slightly shifted ( $\lesssim 2$  GPa) with respect to Table II; this is because of small shifts of the resonant frequencies due to moving the samples from the contact-less laser-based RUS device to the device for field-resolved experiments (Figure 4).

it is apparent that this type of characterization cannot bring similarly detailed insight into the processes in the studied materials and their elastic properties as obtained from temperature-resolved RUS reported above. However, the field-resolved experiments can complement their temperature-resolved counterparts, thereby enabling to qualitatively distinguish between materials with higher and lower levels of residual stresses as well.

### Conflict of Interest

The authors have no conflicts of interest to disclose.



## Data Availability

Raw RUS spectra for all temperature resolved measurements reported in this study are openly available in Zenodo repository at <https://doi.org/10.5281/zenodo.15743726>, reference number 15743726. Other data that support the findings of this study are available from the corresponding author upon reasonable request.

## Acknowledgement

This work received financial support from Czech Science Foundation (GAČR) [projects Nos. 24-10334S and 22-14048S], and from the Czech Ministry of Education, Youth and Sport of the Czech Republic, within the frame of project Ferroic Multifunctionalities (FerrMion) [project No. CZ.02.01.01/00/22\\_008/0004591] co-funded by the European Union.

## REFERENCES

- <sup>1</sup>H. Assadi, H. Kreye, F. Gärtner, T. Klassen, "Cold spraying – A materials perspective," *Acta Mater.* **116**, 382-407 (2016) DOI: 10.1016/j.actamat.2016.06.034
- <sup>2</sup>T. Stoltenhoff, H. Kreye, H.J. Richter, "An analysis of the cold spray process and its coatings," *J. Therm. Spray Technol.* **11**(4), 542 - 550 (2002) DOI: 10.1361/105996302770348682
- <sup>3</sup>A. Papyrin, V. Kosarev, S. Klinkov, A. Alkhimov, V.M. Fomin, *Cold Spray Technology* (Elsevier, Amsterdam, 2007).
- <sup>4</sup>A. Moridi, S.M. Hassani-Gangaraj, M. Guagliano, M. Dao, "Cold spray coating: Review of material systems and future perspectives," *Surf. Eng.* **30**(6), 369 - 395 (2014) DOI: 10.1179/1743294414Y.00000000270
- <sup>5</sup>S. Yin, P. Cavaliere, B. Aldwell, R. Jenkins, H. Liao, W. Li, R. Lupoi, "Cold spray additive manufacturing and repair: Fundamentals and applications," *Addit. Manuf.* **21**, 628 - 650 (2018) DOI: 10.1016/j.addma.2018.04.017
- <sup>6</sup>X. Wang, F. Feng, M.A. Klecka, M.D. Mordasky, J.K. Garofano, T. El-Wardany, A. Nardi, V.K. Champagne, "Characterization and modeling of the bonding process in cold spray additive manufacturing," *Addit. Manuf.* **8** 149 - 162 (2015) DOI: 10.1016/j.addma.2015.03.006
- <sup>7</sup>J. Pattison, S. Celotto, R. Morgan, M. Bray, W. O'Neill, "Cold gas dynamic manufacturing: A non-thermal approach to freeform fabrication," *Int. J. Mach. Tools Manuf.* **47**(3-4), pp. 627 - 634 (2007) DOI: 10.1016/j.ijmachtools.2006.05.001
- <sup>8</sup>C. Borchers, R. Gärtner, T. Stoltenhoff, H. Kreye, "Microstructural bonding features of cold sprayed face centered cubic metals," *J. Appl. Phys.* **96**(8), 4288 - 4292 (2004). DOI: 10.1063/1.1789278
- <sup>9</sup>M. Hassani-Gangaraj, D. Veysset, K.A. Nelson, C.A. Schuh, "In-situ observations of single micro-particle impact bonding," *Scripta Mater.* **145**, 9 - 13 (2018) DOI: 10.1016/j.scriptamat.2017.09.042
- <sup>10</sup>H. Assadi, F. Gärtner, T. Stoltenhoff, H. Kreye, "Bonding mechanism in cold gas spraying," *Acta Mater.* **51**(15) 4379 - 4394 (2003) DOI: 10.1016/S1359-6454(03)00274-X
- <sup>11</sup>J. Xie, D. Nélias, H.W.-L. Berre, K. Ogawa, Y. Ichikawa, "Simulation of the cold spray particle deposition process," *J. Tribol.* **137**(4), 041101 (2015) DOI: 10.1115/1.4030257

- <sup>12</sup>V. Luzin, K. Spencer, M. Zhang, N. Matthews, J. Davis, M. Saleh, "Residual stresses in cold spray coatings," in *Cold-Spray Coatings: Recent Trends and Future Perspectives*, edited by P. Cavaliere, pp. 451 - 480 (2017). DOI: 10.1007/978-3-319-67183-3\_16
- <sup>13</sup>M. Saleh, V. Luzin, K. Spencer, "Analysis of the residual stress and bonding mechanism in the cold spray technique using experimental and numerical methods," *Surf. Coat. Technol.* **252**, 15 - 28 (2014). DOI: 10.1016/j.surfcoat.2014.04.059
- <sup>14</sup>T. Suhonen, T. Varis, S. Dosta, M. Torrell, J.M. Guilemany, "Residual stress development in cold sprayed Al, Cu and Ti coatings," *Acta Mater.* **61**(17), 6329 - 6337 (2013) DOI: 10.1016/j.actamat.2013.06.033
- <sup>15</sup>H. Jahed, R. Ghelichi, "Residual stresses and fatigue life enhancement of cold spray," in *Modern Cold Spray: Materials, Process, and Applications* edited by P. Cavaliere, pp. 225 - 252 (2015) DOI: 10.1007/978-3-319-16772-5\_5
- <sup>16</sup>P. Cavaliere, A. Silvello, "Processing conditions affecting residual stresses and fatigue properties of cold spray deposits," *Int. J. Adv. Manuf. Technol.* **81**(9-12), 1857 - 1862 (2015) DOI: 10.1007/s00170-015-7365-y
- <sup>17</sup>C.M. Sample, V.K. Champagne, A.T. Nardi, D.A. Lados, "Factors governing static properties and fatigue, fatigue crack growth, and fracture mechanisms in cold spray alloys and coatings/repairs: A review," *Addit. Manuf.* **36**, art. no. 101371 (2020) DOI: 10.1016/j.addma.2020.101371
- <sup>18</sup>S.B. Dayani, S.K. Shaha, R. Ghelichi, J.F. Wang, H. Jahed, "The impact of AA7075 cold spray coating on the fatigue life of AZ31B cast alloy," *Surface Coat. Technol.* **337**, 150 - 158 (2018) DOI: 10.1016/j.surfcoat.2018.01.008
- <sup>19</sup>K. Loke, Z.-Q. Zhang, S. Narayanaswamy, P.K. Koh, V. Luzin, T. Gnaupel-Herold, A.S.M. Ang, "Residual Stress Analysis of Cold Spray Coatings Sprayed at Angles Using Through-thickness Neutron Diffraction Measurement" *J. Therm. Spray Technol.* **30**(7), 1810 - 1826 (2021) DOI: 10.1007/s11666-021-01252-5
- <sup>20</sup>S.-H. Park, P. Liu, K. Yi, G. Choi, K.-Y. Jhang, H. Sohn, "Mechanical properties estimation of additively manufactured metal components using femtosecond laser ultrasonics and laser polishing," *Int. J. Mach. Tools Manuf.* **166** 103745 (2021) DOI: 10.1016/j.ijmachtools.2021.103745
- <sup>21</sup>R. Acevedo, P. Sedlak, R. Kolman, M. Fredel "Residual stress analysis of additive manufacturing of metallic parts using ultrasonic waves: State of the art review," *J. Mater. Res. Technol.* **9**(4), 9457 - 9477 (2020) DOI: 10.1016/j.jmrt.2020.05.092
- <sup>22</sup>G. Yamamoto, Y. Sakuda "Determination of elastic constants in complex-shaped materials through vibration-mode-pattern-matching-assisted resonant ultrasound spectroscopy," *J. Appl. Phys.*, **135**(20), art. no. 205109 (2024) DOI: 10.1063/5.0185423
- <sup>23</sup>S.W. Glass, M.R. Larche, M.S. Prowant, J.D. Suter, J.P. Lareau, X. Jiang, K.A. Ross "Cold spray NDE for porosity and other process anomalies," *AIP Conf. Proc.* **1949**, art. no. 020010 (2018) DOI: 10.1063/1.5031507
- <sup>24</sup>O. Hubert, X. Milhet, P. Gadaud, M. Tatat, P.-O. Renault, C. Coupeau "Modeling of Young's modulus variations with temperature of Ni and oxidized Ni using a magneto-mechanical approach," *Mater. Sci. Eng. A* **633**, 76 - 91 (2015) DOI: 10.1016/j.msea.2015.03.014
- <sup>25</sup>R.M. Bozorth, *Ferromagnetism* (D. Van Nostrand, NY, 1951)
- <sup>26</sup>H.M. Ledbetter, R.P. Reed "Elastic Properties of Metals and Alloys, I. Iron, Nickel, and Iron-Nickel Alloys," *J. Phys. Chem. Ref. Data* **2**(3) 531-618 (1973) DOI: 10.1063/1.3253127
- <sup>27</sup>A. Migliori, J.L. Sarrao, W.M. Visscher, T.M. Bell, M. Lei, Z. Fisk, R.G. Leisure, "Resonant ultrasound spectroscopic techniques for measurement of the elastic moduli of solids," *Physica B* **183**(1-2), pp. 1 - 24 (1993) DOI: 10.1016/0921-4526(93)90048-B

- <sup>28</sup>R.G. Leisure, F.A. Willis, "Resonant ultrasound spectroscopy," J. Phys. Condens Matter **9**(28), 6001 - 6029 (1997) DOI: 10.1088/0953-8984/9/28/002
- <sup>29</sup>P. Sedlák, H. Seiner, J. Zídek, M. Janovská, M. Landa, "Determination of All 21 Independent Elastic Coefficients of Generally Anisotropic Solids by Resonant Ultrasound Spectroscopy: Benchmark Examples," Exp. Mech. **54**(6), 1073 - 1085 (2014) DOI: 10.1007/s11340-014-9862-6
- <sup>30</sup>R. Sinclair-Adamson, V. Luzin, A. Duguid, K. Kannoorpatti, R. Murray, "Residual Stress Distributions in Cold-Sprayed Copper 3D-Printed Parts," J. Therm. Spray Technol. **29**(6), 1525 - 1537 (2020) DOI: 10.1007/s11666-020-01040-7
- <sup>31</sup>H. Seiner, J. Cizek, P. Sedlák, R. Huang, J. Cupera, I. Dlouhy, M. Landa, "Elastic moduli and elastic anisotropy of cold sprayed metallic coatings," Surf. Coat. Technol. **291**, 342 - 347 (2016) DOI: 10.1016/j.surfcoat.2016.02.057
- <sup>32</sup>J. Cizek, O. Kovarik, J. Cupera, J. Kondas, T. Bajer, F. Siska, M. Janovska, H. Seiner, "Measurement of mechanical and fatigue properties using unified, simple-geometry specimens: Cold spray additively manufactured pure metals," Surf. Coat. Technol. **412**, 126929 (2021) DOI: 10.1016/j.surfcoat.2021.126929
- <sup>33</sup>J.T. Houston, K. Farrell, "Recrystallization of nickel-270," Metallogr. **2**(2-3), 239 - 246 (1969) DOI: 10.1016/0026-0800(69)90086-X
- <sup>34</sup>J. Nejezchlebová, H. Seiner, M. Ševčík, M. Landa, M. Karlík "Ultrasonic detection of ductile-to-brittle transitions in free-cutting aluminum alloys" (2015) NDTE Int. **69**, 40 - 47 (2015) DOI: 10.1016/j.ndteint.2014.09.007
- <sup>35</sup>H. Seiner, P. Sedlák, L. Bodnárová, J. Drahokoupil, V. Kopecký, J. Kopeček, M. Landa, O. Heczko, "The effect of antiphase boundaries on the elastic properties of Ni-Mn-Ga austenite and premartensite," J. Phys. Condens. Matter. **25**(42) 425402 (2013) DOI: 10.1088/0953-8984/25/42/42
- <sup>36</sup>C.A. Mizzi, B. Maiorov, "Enabling resonant ultrasound spectroscopy in high magnetic fields," J. Acoust. Soc. Am. **155**(5), 3505 – 3520 (2024) DOI: 10.1121/10.0026124
- <sup>37</sup>R. Singh, J. Kondás, C. Bauer, J. Cizek, J. Medricky S. Csaki, J. Čupera, R. Procházka R., D. Melzer P. Konopík, "Bulk-like ductility of cold spray additively manufactured copper in the as-sprayed state," Add. Manuf. Lett., **3** 100052 (2022) DOI: 10.1016/j.addlet.2022.100052
- <sup>38</sup>Y. Zou, W. Qin, E. Irissou, J.-G. Legoux, S. Yue, J.A. Szpunar, "Dynamic recrystallization in the particle/particle interfacial region of cold-sprayed nickel coating: Electron backscatter diffraction characterization," Scripta Mater. **61**(9) 899 – 902 (2009) DOI: 10.1016/j.scriptamat.2009.07.020
- <sup>39</sup>A.S. Nowick, B.S. Berry, *Anelastic Relaxation in Crystalline Solids* (Academic Press, New York. 1972)
- <sup>40</sup>M. Koller, P. Sedlák, H. Seiner, M. Ševčík, M. Landa, J. Stráská, M. Janeček, "An ultrasonic internal friction study of ultrafine-grained AZ31 magnesium alloy," J. Mater. Sci. **50**(2), 808 – 818 (2014) DOI: 10.1007/s10853-014-8641-1
- <sup>41</sup>J. Cizek, J. Medricky, F. Stefanik, F. Lukac, J. Cupera, J. Kondas, R. Singh, O. Melikhova, P. Hruska, J. Cizek, "Cold Sprayed Deposits Characterized by Positron Annihilation Spectroscopy," J. Therm. Spray Technol. **33**(2-3) 666 - 675 (2024) DOI: 10.1007/s11666-024-01763-x
- <sup>42</sup>J.A. Benito, J.M. Manero, J. Jorba, A. Roca, "Change of Young's modulus of cold-deformed pure iron in a tensile test," Metall. Mater. Trans. A **36**(12), 3317 - 3324 (2005) DOI: 10.1007/s11661-005-0006-6

- <sup>43</sup>H.Y. Yu, "Variation of elastic modulus during plastic deformation and its influence on spring-back," *Mater. Des.* **30**(3), 846 - 850 (2009) DOI: 10.1016/j.matdes.2008.05.064
- <sup>44</sup>K. Yamaguchi, H. Adachi, N. Takakura, "Effects of plastic strain and strain path on Young's modulus of sheet metals," *Met. Mater. Int.* **4**(3), 420 - 425 (1998) DOI: 10.1007/bf03187802
- <sup>45</sup>A. Yoneda, "Intrinsic eigenvibration frequency in the resonant ultrasound spectroscopy: Evidence for a coupling vibration between a sample and transducers," *Earth PLanets Space* **54**(7), 763 - 770 (2002) DOI: 10.1186/BF03351729
- <sup>46</sup>S.J. Reese, K.L. Telschow, T.M. Lillo, D.H. Hurley "On the establishment of a method for characterization of material microstructure through laser-based resonant ultrasound spectroscopy," *IEEE Trans. Ultrason. Ferroelectr. Freq. Control*, **55**(4), 770 - 776 (2008) DOI: 10.1109/TUFFC.2008.711